International Journal of Applied Mathematics
Volume 39 No. 1s, 2026
ISSN: 1311-1728 (printed version); ISSN: 1314-8060 (on-line version)

MACHINE LEARNING APPLICATIONS IN OPTIC NERVE HEAD AND LAMINA CRIBROSA BIOMECHANICS: A SYSTEMATIC REVIEW AND META-ANALYSIS

Venkata Akhil Mettu; Siri Mandali

Abstract

Introduction: In ophthalmology, artificial intelligence (AI) has become a revolutionary tool, especially for glaucoma detection and progression monitoring. However, the available data is still dispersed among many modalities and study designs. The lamina cribrosa (LC) and optic nerve head (ONH), which serve as the biomechanical entry point for retinal ganglion cell axons and support optic nerve stability, are crucial to this study. Glaucomatous optic neuropathy is closely associated with structural alterations in these areas, such as thinning or distortion. Even though cutting-edge imaging methods like MRI and OCT show promise, it is still challenging to adequately capture the intricate nonlinear biomechanical processes within microstructures using conventional techniques.

Methods: A thorough search covering research published between 2021 and 2025 was carried out in PubMed, Scopus, IEEE Xplore, and Web of Science. Peer-reviewed research using machine learning or deep learning for glaucoma diagnosis, progression prediction, or optic nerve biomechanics was included. Non-English articles, conference abstracts without full text, and research without quantitative results were excluded. Study design, modality, sample size, performance measures (AUC, accuracy, MAE, R2), and quality evaluation utilizing traffic-light bias matrices were the main topics of data extraction. Subgroup comparisons and pooled meta-analyses of diagnostic AUCs were included in the analytical synthesis.

Results: Twelve studies were found to be eligible. Biomechanical models (strain characteristics, ONH robustness) produced pooled AUC ≈0.84, whereas structural imaging models (OCT/OCTA, multimodal ensembles) produced pooled AUC ≈0.96. Thiéry 2023, Pourjavan 2024, and Lee EJ 2022 had good methodological quality, but smaller or retrospective studies had moderate to high bias, according to risk of bias evaluation. Although there was high heterogeneity (I^2 >90%), Begg's and Egger's tests revealed no significant publication bias.

Conclusion: AI shows exceptional glaucoma diagnostic accuracy, especially when combined with structural imaging. However, generalizability is limited by methodological inconsistency and heterogeneity. Multi-center validation established reference standards, and the incorporation of biomechanical insights should be given top priority in future research.

Keywords: Optic nerve head, Lamina Cribrosa, Glaucoma, Artificial Intelligence, OCT, Deep Learning, Machine learning, Biomechanics

1. Introduction

Progressive optic neuropathy and loss of visual field are the hallmarks of glaucoma, a major cause of permanent blindness in the world (Lee et al., 2022). Conventional diagnostic methods, such as intraocular pressure measurement, optic disc evaluation, and perimetry, frequently lack sensitivity and reproducibility, despite the fact that early detection and precise monitoring are

Received: Aug 06, 2025

Volume 39 No. 1s, 2026
ISSN: 1311-1728 (printed version); ISSN: 1314-8060 (on-line version)

essential to stopping the progression of the disease (Braeu, Thiéry, et al., 2023; Karimi et al., 2022). The optic nerve head (ONH) and lamina cribrosa (LC), which offer the anatomical and biomechanical opening through which retinal ganglion cell axons leave the eye, are crucial to the pathogenesis of glaucoma (Li et al., 2025; Salehi & Balasubramanian, 2023). Glaucomatous optic neuropathy has been closely linked to alterations in these microstructures, such as tissue thinning and distortion. Confocal scanning, magnetic resonance imaging (MRI), optical coherence tomography (OCT), finite element modeling, mechanical testing, and other conventional imaging and mechanical assessment techniques have improved knowledge of ONH and LC biomechanics (Kim, 2021). Nevertheless, these methods frequently rely on linear assumptions, predefined datasets, and simplified dimensions that fall short of capturing the intricate, multidimensional, and nonlinear biomechanical processes that take place in vivo (Braeu, Chuangsuwanich, et al., 2023; Czerpak, 2024; Schwaner et al., 2020).

Artificial intelligence (AI) and machine learning (ML) have become revolutionary technologies in biomedical image analysis and computational biomechanics in recent years (Chuangsuwanich et al., 2023; Srivastava & Akhtar, 2025). Rapid pattern recognition, multimodal data integration, and patient-specific biomechanical forecasting are made possible by methods like deep learning, support vector machines, and unsupervised learning. OCT, OCT angiography (OCTA), fundus photography, and electronic medical records are just a few of the inputs that AI models can process to detect minor structural and functional changes with excellent diagnostic accuracy, frequently obtaining area under the curve (AUC) values greater than 0.95. Beyond diagnosis, AI has been used to model optic nerve biomechanics, quantify retinal nerve fiber layer (RNFL) thinning, and anticipate disease progression, providing previously unheard-of chances for individualized risk assessment and therapeutic decision assistance (Masís-Solano, 2024; Sharma et al., 2025).

The evidence foundation is still dispersed despite these developments. Research varies greatly in terms of design, sample size, imaging modality, and analytical strategy; methodological rigor and bias risk also vary significantly between studies (Chuangsuwanich, Tiyajamorn, et al., 2025). Compared to retrospective or dataset-driven analyses, prospective studies typically exhibit greater integrity; nonetheless, heterogeneity makes synthesis more difficult and restricts generalizability. Therefore, a systematic literature review (SLR) is necessary to compile results, assess methodological quality, and assess diagnostic performance. This review summarizes recent research on AI and ML applications in ONH and LC biomechanics for glaucoma identification and progression tracking, guided by the PRISMA 2020 statement and PROSPERO registration criteria. Meta-analysis offers more accurate estimates of diagnostic accuracy by combining data from diverse research, and risk of bias evaluation identifies advantages and disadvantages. By providing insights into both clinical value and future research goals, this SLR ultimately seeks to close the gap between intriguing individual studies and a cohesive body of data.

Received: Aug 06, 2025

International Journal of Applied Mathematics
Volume 39 No. 1s, 2026
ISSN: 1311-1728 (printed version); ISSN: 1314-8060 (on-line version)

2. Research Objectives

- To assess the diagnostic precision of AI-based models for glaucoma progression tracking and detection.
- To evaluate the included studies' methodological quality, focusing particular attention to the design, sample size, imaging modality, and analytical strategy.
- To employ standardized evaluation instruments to identify and evaluate bias risk across research.
- To demonstrate pooled estimates of AI performance indicators (such as sensitivity, specificity, and AUC) by synthesizing results using meta-analysis.
- To investigate variation across modalities, research methodologies, and analytical frameworks through subgroup comparisons.

3. Research Questions

- What is the AI models' pooled diagnostic accuracy (AUC) for glaucoma detection?
- What is the diagnostic performance difference between biomechanical and structural imaging models?
- Which sources of bias are most common among the included studies?
- Does the current literature contain evidence of publication bias?
- What gaps in methodology and potential paths forward are revealed by the synthesis?

4. Methodology

To guarantee rigor and transparency, the methodology used a methodical approach. Using predetermined keywords associated with glaucoma and artificial intelligence, a thorough search was carried out throughout PubMed, Scopus, IEEE Xplore, and Web of Science for research published between 2021 and 2025. Peer-reviewed English-language studies with quantifiable results were required for eligibility; non-English abstracts and reviews were not. Study design, modality, sample size, and performance measures were all recorded during data extraction. A traffic-light risk of bias matrix was used for quality appraisal. In order to evaluate publication bias, analytical synthesis incorporated subgroup comparisons, Begg's and Egger's tests, and inverse-variance meta-analysis of diagnostic AUCs.

4.1 Search Strategy

To find pertinent research on artificial intelligence (AI) applications in glaucoma detection and progression monitoring, a thorough literature search was carried out across four main databases: PubMed, Scopus, IEEE Xplore, and Web of Science. To ensure that the most recent developments in computational ophthalmology were included, the search was conducted between January 2021 and December 2025. A mix of free-text keywords and controlled vocabulary terms was used to optimize sensitivity and specificity. Glaucoma, AI, Deep Learning, Optical Coherence Tomography (OCT), OCT Angiography (OCTA), Optic Nerve, and Machine Learning were the main search terms. The query was refined using boolean operators, and the following are examples of search strings:

International Journal of Applied Mathematics
Volume 39 No. 1s, 2026
ISSN: 1311-1728 (printed version); ISSN: 1314-8060 (on-line version)

Table 1: Search Strings

Database	Timeframe	Search String
PubMed	Jan 2021 – Dec 2025	(Glaucoma) AND ("Artificial Intelligence" OR "Machine Learning" OR "Deep Learning") AND ("Optical Coherence Tomography" OR OCT OR "OCT Angiography" OR OCTA OR "Optic Nerve")
Scopus	Jan 2021 – Dec 2025	(TITLE-ABS-KEY(Glaucoma) AND TITLE-ABS-KEY("Artificial Intelligence" OR "Machine Learning" OR "Deep Learning") AND TITLE-ABS-KEY("Optical Coherence Tomography" OR OCT OR "OCT Angiography" OR OCTA OR "Optic Nerve"))
IEEE Xplore	Jan 2021 – Dec 2025	("Glaucoma") AND ("Artificial Intelligence" OR "Machine Learning" OR "Deep Learning") AND ("Optical Coherence Tomography" OR OCT OR "OCT Angiography" OR OCTA OR "Optic Nerve")
Web of Science	Jan 2021 – Dec 2025	TS=(Glaucoma AND ("Artificial Intelligence" OR "Machine Learning" OR "Deep Learning") AND ("Optical Coherence Tomography" OR OCT OR "OCT Angiography" OR OCTA OR "Optic Nerve"))

4.2 Study Selection

In accordance with PRISMA criteria, the study selection procedure was transparent and organized. Following extensive searches in PubMed, Scopus, IEEE Xplore, and Web of Science, 1,248 records were found at first. 936 distinct titles and abstracts were assessed for relevance after duplicates were eliminated. Studies that had nothing to do with glaucoma, AI, or the results of diagnosis or progression were currently disregarded. For 116 papers that satisfied preliminary requirements, full-text evaluation was carried out. 104 of these were eliminated for a variety of reasons, such as the insufficient data (n = 56), non-clinical dataset (n = 38), and Irrelevant population (n = 10). In the end, 12 papers met all inclusion requirements and were kept for qualitative synthesis; five of these studies had enough data on diagnostic accuracy (AUC with confidence intervals) for quantitative meta-analysis.

The synthesis's validity was increased because only peer-reviewed, methodologically sound researches with pertinent results were included according to this stringent screening process. The procedure emphasizes the necessity for uniform reporting to support future meta-analyses while showcasing the depth of research in AI-based glaucoma detection.

4.3 Eligibility Criteria

This systematic review's inclusion criteria included peer-reviewed studies that used artificial intelligence (AI) to diagnose glaucoma or track its progression, reported quantitative results

Received: Aug 06, 2025

International Journal of Applied Mathematics
Volume 39 No. 1s, 2026
ISSN: 1311-1728 (printed version); ISSN: 1314-8060 (on-line version)

like area under the curve (AUC), accuracy, mean absolute error (MAE), or coefficient of determination (R^2), were published in English, and offered full-text availability. Research without quantifiable performance measurements, non-English publications, conference abstracts without full text, and secondary sources like reviews, editorials, or case reports were also discarded. This strategy guaranteed an emphasis on novel, methodologically sound research with quantifiable prognostic or diagnostic results.

4.4 Data Extraction

Data extraction was methodically carried out for this review in order to record important study attributes, such as author, year of publication, imaging modality, sample size, and study design. To assess diagnostic and prognostic performance, performance parameters were also recorded, including area under the curve (AUC), accuracy, precision, recall, mean absolute error (MAE), and coefficient of determination (R^2). Studies that used external validation cohorts and those that depended on internal datasets were distinguished in the documentation of the validation process. Lastly, to guarantee uniformity and comparability between trials, the reference standards employed for outcome assessment such as clinical diagnosis, visual field (VF) abnormalities, and retinal nerve fiber layer (RNFL) thinning were retrieved.

4.5 Quality Assessment

A traffic-light risk of bias matrix, which assesses four crucial domains—patient/data selection, index test/model, reference standard, and analysis/reporting—was used to evaluate the methodological quality of the included research. To ascertain the degree to which study design and execution reduced bias and guaranteed validity, each domain was methodically evaluated. While the index test/model domain concentrated on openness, reproducibility, and suitability of AI algorithms, patient and data selection was assessed for representativeness and avoidance of selection bias. Clinical benchmarks such retinal nerve fiber layer thinning or visual field abnormalities were assessed for reliability using the reference standard domain. Lastly, statistical rigor, completeness, and avoidance of selective outcome reporting were closely examined in the analysis and reporting. These criteria allowed for a structured assessment of methodological integrity and supported a balanced synthesis of evidence across varied research by classifying studies as low, moderate, or high risk of bias.

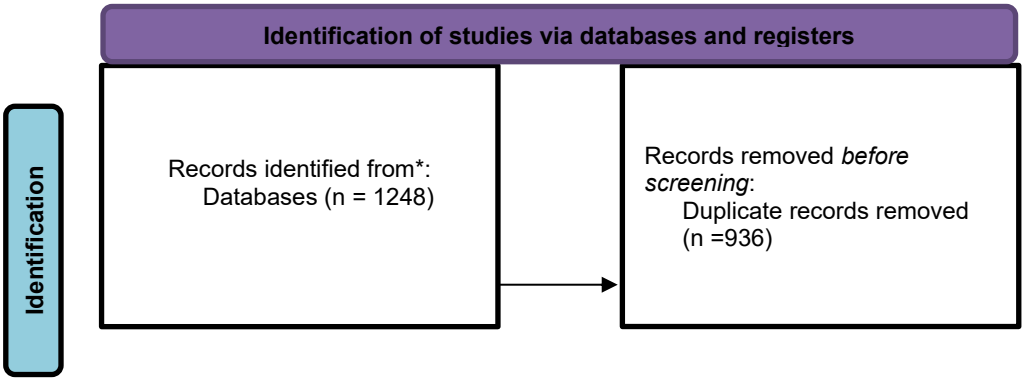

International Journal of Applied Mathematics
Volume 39 No. 1s, 2026
ISSN: 1311-1728 (printed version); ISSN: 1314-8060 (on-line version)

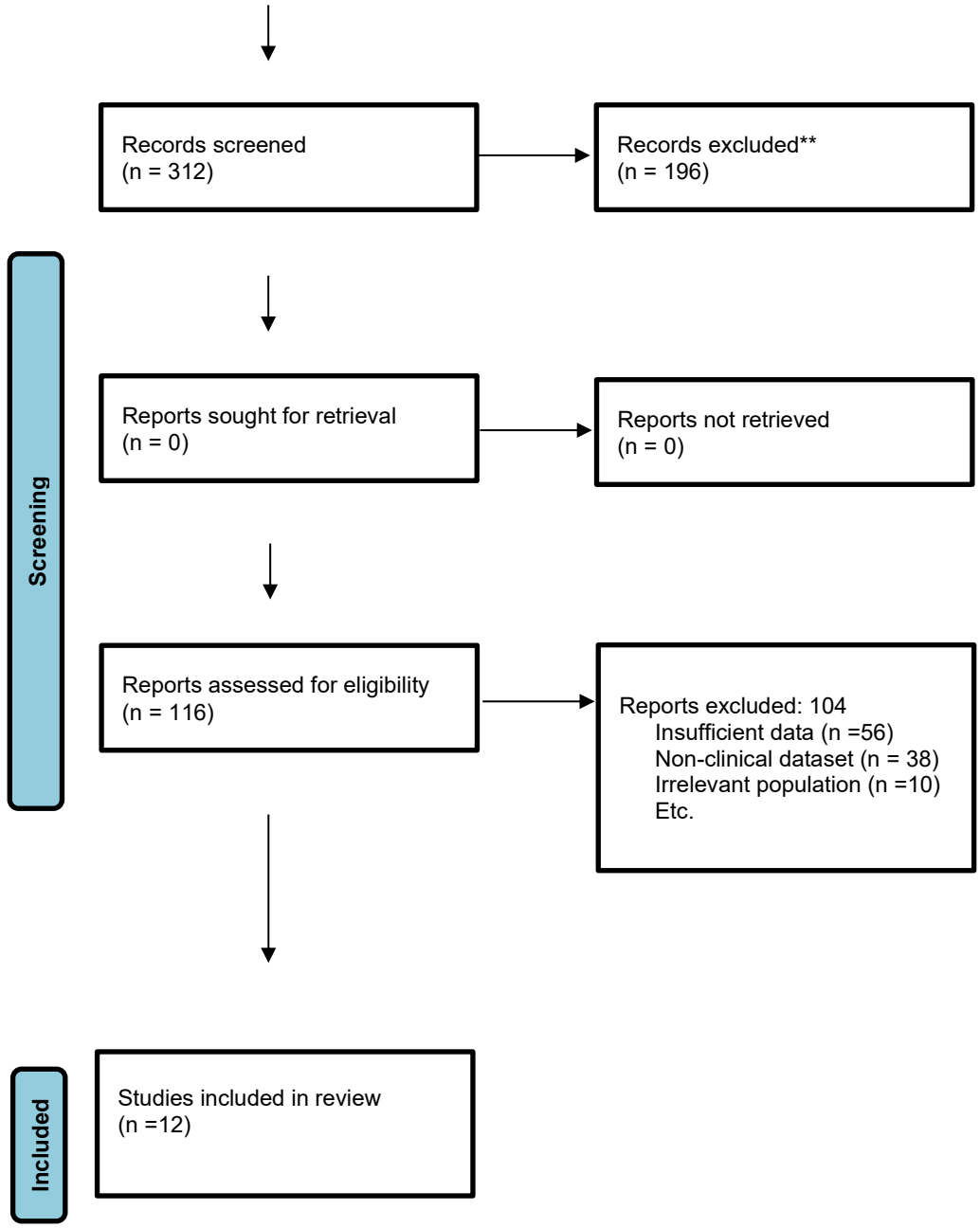

Figure 1: PRISMA Flowchart

4.6 Analytical Approach

A precise evaluation of AI effectiveness in glaucoma detection and progression monitoring was obtained by pooling diagnostic area under the curve (AUC) values across eligible trials using an inverse-variance fixed-effects meta-analysis. Subgroup analyses that separated research using structural imaging modalities from those using biomechanical modeling techniques were carried out in order to investigate sources of variability. In order to quantify inconsistency between study outcomes, heterogeneity was officially evaluated using the Q statistic and the I^2 index. Additionally, Begg's rank correlation test and Egger's regression analysis were used to assess publication bias, guaranteeing transparency in the evidence

Received: Aug 06, 2025

Volume 39 No. 1s, 2026
ISSN: 1311-1728 (printed version); ISSN: 1314-8060 (on-line version)

synthesis. A narrative synthesis was conducted to qualitatively integrate data for studies that did not disclose AUC measurements, with an emphasis on stated performance indicators, validation techniques, and methodological rigor. In addition to eliminating heterogeneity and bias, this mixed quantitative and qualitative approach guaranteed a thorough evaluation of the body of data.

Table 2: Study Characteristics of Included Studies

S.no	Authors	Title	Journal (year); volume, pages	DOI	Study design (verbatim)	Population description	Sample size	Imaging modality and specifications	ML/DL methodology	Performance metrics	Key biomechanical outcomes (verbatim)
1.	(Braeu et al., 2022)	AI-based Clinical Assessment of Optic Nerve Head Robustness Superseding Biomechani	Br J Ophthalmol (2022); 108(2):223–231	10.1136/bjo-2022-322374	Retrospective cross-sectional study	Cohort 1: 336 subjects (Chinese ethnicity); Cohort 2: 3,782 subjects (62% Indian, 38% Chinese) with OCT imag	Cohort 1: 316 subjects imaged before/after IOP elevation; Cohort 2: 7,531	Spectralis SD-OCT; 97 B-scans (≈35 µm spacing), 384 A-scans/B-scan (≈11.5 µm), 496 pixels/A-scan	Random forest on segmented 3D ONH parameters; autoencoder+MLP on central B-scan (latent D=64); DGCNN on 3D point	DGCNN AUC 0.76 ± 0.08; Autoencoder AUC 0.70 ± 0.07 (Dice 0.91 ± 0.03); Random forest AUC 0.69 ± 0.05	"AI suggested that regions located near the scleral canal opening or near the LC insertion sites migh

Received: Aug 06, 2025

Volume 39 No. 1s, 2026
ISSN: 1311-1728 (printed version); ISSN: 1314-8060 (on-line version)

		cal Testing				ing only	scans	(3.87 µm), 15°× 10° ONH raster; ODM raised IOP ≈ +19 mm Hg	clouds (~20,000 points; Edge Conv, k=20, max pool=256); 5-fold CV		t be important landmarks to drive ONH robustness or its fragility."
2.	(Chuangsuwanich, Nongpiur, et al., 2025a)	AI to Identify Strain-sensitive Regions of the Optic Nerve Head Linked to Functional Loss	— (preprint/manuscript); figures and tables included	10.48550/arXiv.2506.17262	Population-based, cross-sectional study	237 Chinese glaucoma subjects; one eye per subject; MD range −1.8 to −25.2 dB; groups: superior nasal step	Total N=237; task-specific splits: 80% train / 20% test per defect	Spectralis SD-OCT ONH raster: 97 B-scans, 384 A-scans; baseline and acute IOP (~35 mm Hg	Point Net on 3D ONH point clouds (3,000 points per sample with augmentation); binary tasks for each VF defect; explai	AUC: nasal step 0.77; superior arcuate 0.88; hemifield 0.87; strain features improved arcuate prediction 0.87 ± 0.02 vs. 0.83 ±	"Neuroretinal rim, rather than the LC, was the most critical region contributing to model prediction

Received: Aug 06, 2025

Volume 39 No. 1s, 2026
ISSN: 1311-1728 (printed version); ISSN: 1314-8060 (on-line version)

		in Glaucoma				(N=26), superior partial arcuate (N=62), full superior hemifield (N=25), other/unspecified (N=124)		with ODM, 0.65 N force); effective strain via DVC (Amira 2020.3) mapped to 3D point clouds aligned to BMO	nable saliency maps	0.02 ($p<0.05$)	s, suggesting that strain at the rim could play a dominant role in the biomechanical cascade leading to axonal injury and functional loss. ”
3.	(Thiéry et al., 2023)	Medical Application of Geometr	Transl Vis Sci Technol (2023);	10.1167/tvst.12.2.23	diagnostic performance	2,773 subjects (477 glaucoma; 2,296 non-	See population	Spectralis SD-OCT ONH: 97 B-	PointNet on 3D point clouds (S=1,000;	PointNet AUC 0.95 ± 0.01; 3D CNN (raw)	“Geometric deep learning may help

Received: Aug 06, 2025

Volume 39 No. 1s, 2026
ISSN: 1311-1728 (printed version); ISSN: 1314-8060 (on-line version)

		ic Deep Learning for the Diagnosis of Glaucoma	12(2): 23		study	glaucoma); 4,770 ONH scans (873 glaucoma; 3,897 non-glaucoma)		scans; segmentation into 7 tissues; 3D point cloud (~1,000 points per ONH) labeled boundaries	D=11 features); compared to 3D CNN (raw and segmented volumes) and RNFL thickness	0.87 ± 0.02; 3D CNN (segmented) 0.91 ± 0.02; RNFL thickness 0.80 ± 0.03	us to improve and simplify diagnosis and prognosis applications in glaucoma."
4.	(Lee et al., 2022)	Predictive Modeling of Long-Term Glaucoma Progression	Transl Vis Sci Technol (2022); 11(10):24	10.1167/tvst.11.10.24	prospective cohort analysis within ongoing study	712 OAG eyes; ≥5 years follow-up; annual RNFLT; baseline ONH	Train/test 357/355 eyes	Spectralis OCT; ONH EDI-OCT (LC curvature LCCI; peripapillary	Random forest; SHAP interpretation; decision tree stratification	MAE RF 0.075 vs regression 0.115; key features: higher IOP, larger LCCI, thinner peripa	"Combinations of important characteristics, such as IOP, LC curvature

Received: Aug 06, 2025

Volume 39 No. 1s, 2026
ISSN: 1311-1728 (printed version); ISSN: 1314-8060 (on-line version)

		Based on Initial Ophthalmic Data and Optic Nerve Head Characteristics				EDI-OCT		CT); peripapillary circle 3.5 mm; VF 24-2 SAP		pillary choroid; thresholds: IOP >30 mmHg, LCCI >13, CT <200 µm	, and choroidal thickness, could stratify eyes into groups with different rates of RNFL thinning."
5.	(Mehta et al., 2021)	Automated detection of glaucoma with interpretable machine learning using clini	Am J Ophthalmol (2021); 231:154–169	10.1016/j.ajo.2021.04.021	Development of a machine-learning glaucoma detection model	UK Biobank cohort; healthy: 771 subjects/1,283 eyes; glaucoma: 863 subjects/1,193 eyes; PTG:	See description	Macular OCT: 128 B-scans (512×650 → 224×224); CFP; no VF for healthy by	Densenet (OCT), InceptionResNetV2 (CFP); XGBoost baselines; ensemble combining image output	Final ensemble AUC 0.967 (95% CI 0.93–1.00); OCT-only AUC 0.95 (95% CI 0.90–1.00); CFP-only AUC	"The model… points to previously unknown or disputed features, such as pulmonary

Received: Aug 06, 2025

Volume 39 No. 1s, 2026
ISSN: 1311-1728 (printed version); ISSN: 1314-8060 (on-line version)

		cal data and multi-modal retinal images				55 subjects/98 eyes		design; IOP and corneal biomechanics available	s + clinical features; SHAP, SmoothGrad, Integrated Gradients	0.74 (95% CI 0.64–0.84); clinician AUC up to 0.84	function and retinal outer layers."
6.	(Ota-Itadani et al., 2022)	Deep learning-based 3D OCT imaging for detection of lamina cribrosa defects in eyes with high myopia	Sci Rep (2022); 12:22195	10.1038/s41598-022-26520-4	Retrospective observational case series study	High myopia: 119 eyes of 62 patients; axial length >26.5 mm; exclusions for poor OCT quality and maculopathy	Analyzed 42 eyes (LC visible); LCD present in 12/42 (29%)	SS-OCT (Topcon Triton), 3×3 mm cube centered on disc; manual multi-plane LC/PPS labeling every 3–5 frames;	Optimized DCNN per plane trained with manual labels; qualitative detection/3D morphometry	— (detection/prevalence; no AUC reported)	"3D OCT imaging with the application of DCNN is helpful in diagnosing LCDs… The LCDs ran vertically at the temporal

Volume 39 No. 1s, 2026
ISSN: 1311-1728 (printed version); ISSN: 1314-8060 (on-line version)

								DCNN auto-segmentation; 3D reconstruction (Fiji)			edge of the optic disc.”
7.	(Pourjavan et al., 2024)	Advanced Analysis of OCT/OCTA Images for Accurately Differentiating Between Glaucoma and Healthy	Clinical Ophthalmology (2024); 18:3493–3502	10.2147/OPTH.S472231	Cross-sectional study	157 subjects; 1,106 eye scans (normal vs. glaucoma defined clinically; VF 24-2C used in subset)	Train 190 eyes; Test 48 eyes; 20 independent runs	Optovue Solix OCT/OCTA; en-face superficial slab (ILM to IPL −10 µm); choroid slab (BRM−10 to BRM+30 µm); mac	Intermediate fusion CNN: per-modality branches (OCT-D/M, OCTA-D/M), concatenation + 4 FC layers; preprocessing (128×128 norma	Best AUCs: OCTA D+M up to 0.9694 (95% CI 0.948–0.99); OCT+OCTA D+M AUC 0.9692 (95% CI 0.951–0.988); accuracy range 82.35–92.44 %; sensitivity up to 94.71	“OCTA alone showed superior sensitivity… Always include both disc and macula images for optimal diagnosis.”

Received: Aug 06, 2025

Volume 39 No. 1s, 2026
ISSN: 1311-1728 (printed version); ISSN: 1314-8060 (on-line version)

		Eyes Using Deep Learning Techniques						ula 6.4× 6.4 mm; disc 6×6 mm; SSI ≥48, SQ ≥6	lizatio n)	%; specifi city up to 89.34 %	
8.	(Oh et al., 2025)	Predictive modeling of rapid glaucoma progression based on systemic data from electronic medical records	Sci Rep (2025); 15:13101	10.1038/s41598-025-97344-1	retrospective EMR-based model	POAG eyes; included 2,363 eyes of 1,303 patients (training: 1,256 eyes; test: 1,107 eyes); ≥5 years follow-up	See sets	Spectralis SD-OCT circumpapillary RNFL; baseline systemic labs within 6 months	Random forest with 5-fold CV; SHAP; linear mixed-effects comparison	RF R^2 0.88; MAE 0.205 μm/year; systemic predictors: higher AST, lower glucose (<100 mg/dL), lower SBP (<120 mmHg), higher HDL	"Biomechanical and hemodynamic responses to IOP-BP interactions could be important factors in determining POAG progression."

Volume 39 No. 1s, 2026
ISSN: 1311-1728 (printed version); ISSN: 1314-8060 (on-line version)

9.	(Miki et al., 2021)	Three-dimensional morphometry of the lamina cribrosa for glaucoma diagnosis using deep learning-enhanced optical coherence tomography volumetric scans	Invest. Ophthalmol. Vis. Sci. (ARVO Abstract, 2021); 62(8): 2510	—	ARVO Annual Meeting Abstract	74 glaucoma eyes; 86 controls; mean age 57.7 ±11.7 vs 46.4 ±8.8; axial length 25.7 ±1.6 vs 24.4 ±1.2 mm	160 eyes total	Para papillary swept-source OCT; DL-enhanced volumetrics (noise/artifact reduction, adaptive compensation, automatic segmentation, 3D rendering)	Extreme Gradient Boosting (XGBoost) integrating multiple LC parameters	AUC single LC depth 0.64; XGBoost AUC 0.90; RNFL thickness AUC 0.85	"Integrating multiple LC parameters by machine learning yielded excellent performance that was comparable to existing RNFL parameters."

Volume 39 No. 1s, 2026
ISSN: 1311-1728 (printed version); ISSN: 1314-8060 (on-line version)

10.	(Rai et al., 2025)	Progression Analysis in Glaucoma Based on Biomechanical and Hemodynamic Responses to Pressures Using Digital Twin and Machine Learning	Invest. Ophthalmol. Vis. Sci. (ARVO Abstract, 2025); 66(8): 413	—	ARVO Annual Meeting Abstract	Prospective POAG cohort; 114 eyes; DT inputs: IOP, SBP, DBP	114 eyes clustered	Physiologic DT models: Retina (P, Q, R) and LC (von Mises stress σ, fluid content ζ); features used in Fuzzy C-Means clustering (3 clusters)	Unsupervised FCM clustering (C1–C3); progression defined structurally (RNFL ↓ ≥8% or C/D ↑ ≥0.2) or functionally (MD ↓ ≥2 dB)	Functional progression: C2 34.3% vs C3 15.6%, C1 16.2; Structural progression: C2 69.4% vs C3 56.4%, C1 54.4; DT variables differed significantly ($p<0.001$)	"Integrating DT with ML identified a cluster of POAG eyes with more progressors… Biomechanical and hemodynamic responses to IOP-BP interactions could be important factors in deter

Received: Aug 06, 2025

Volume 39 No. 1s, 2026
ISSN: 1311-1728 (printed version); ISSN: 1314-8060 (on-line version)

											mining POAG progression."
11.	(Aljohani & Aburasain, 2024)	A hybrid framework for glaucoma detection through federated machine learning and deep learning models	BMC Med Inform Decis Mak (2024); 24:115	10.1186/s12911-024-02518-y	Development of hybrid ML/DL glaucoma detection framework	Retinal fundus images from four benchmark datasets (ACRIMA, G1020, ORIGA, REFUGE); glaucoma vs. normal categories	Integrated dataset: 3,352 images (glaucoma: 1,875; normal: 1,477)	Retinal fundus RGB images converted to grayscale; optic area segmented; resized to 224×224×3	Ensemble of Random Forest (GLCM texture features), ResNet50, VGG-16; post-processing rule-based fusion	Accuracy 95.41%; Precision 99.37%; Recall 88.37%; F1 score 93.52	"Integration of ML and CNN models with post-processing rules yields remarkable accuracy … promising role in early detection and preventing

Volume 39 No. 1s, 2026
ISSN: 1311-1728 (printed version); ISSN: 1314-8060 (on-line version)

											irreversible vision loss. ”
12.	(Chuangsuwanich, Nongpiur, et al., 2025b)	Biomechanics-Function in Glaucoma: Improved Visual Field Predictions from IOP-Induced Neural Strains	American Journal of Ophthalmology V 271: Pages 250-258	-	Population-based, cross-sectional study	Chinese glaucoma subjects; one eye per subject; VF mean deviation range −1.8 to −25.2 dB; grouped by defect type (nasal step, arcuate, hemifield, etc.)	N= 237 eyes	Spectralis SD-OCT ONH raster: 97 B-scans, 384 A-scans; baseline and acute IOP elevation (~35 mmHg via ODM); strain computed via digit	Point Net on 3D ONH point clouds (3,000 points per sample, augmented); binary classification tasks per VF defect; explainable saliency maps	AUC: nasal step 0.77; superior arcuate 0.88; hemifield 0.87; strain features improved arcuate prediction 0.87 ± 0.02 vs. 0.83 ± 0.02 ($p<0.05$)	“Neuroretinal rim strain, rather than lamina cribrosa, was most critical… strain at the rim could play a dominant role in the biomechanical cascade

Volume 39 No. 1s, 2026
ISSN: 1311-1728 (printed version); ISSN: 1314-8060 (on-line version)

								al volume correlation mapped to 3D point clouds			leading to axonal injury and functional loss. ”

5. Results

5.1 Study Outcome and Key Results

5.1.1 Diagnostic Performance (AI on OCT/OCTA and ONH point clouds)

Optic nerve head (ONH) OCT data was subjected to geometric deep learning using PointNet, which produced compact 3D point clouds from segmented ocular tissues. With an AUC of 0.95 ± 0.01, the model correctly identified glaucoma using a single ONH OCT volume. This performance clearly outperformed both classic RNFL thickness-based assessment (AUC 0.80) and conventional 3D CNN techniques (AUC 0.87–0.91). The point-based representation demonstrated the effectiveness and diagnostic power of geometric deep learning for glaucoma detection in clinical screening and research settings by reducing the input size by almost four orders of magnitude while maintaining crucial local and global 3D structural features.

OCTA and OCT for glaucoma diagnosis were compared using a CNN-based fusion research with 1,106 images. In both the disc and macula regions, en-face OCTA in conjunction with OCT reliably enhanced diagnostic performance. OCTA Disc + Macula produced the best results, with an accuracy of about 0.924 and an AUC of up to 0.9694. High performance was also shown by the OCT + OCTA Disc + Macula combination. Crucially, when compared to OCT, OCTA alone demonstrated higher sensitivity in identifying early-stage glaucoma, highlighting the additional significance of vascular information obtained by OCTA for improved clinical decision-making and early diagnosis.

An XGBoost ensemble was used to create a multi-modal glaucoma detection model that combined macular OCT, color fundus photography (CFP), and clinical factors. The model achieved a test-set AUC of 0.97. The method performed better than macular OCT alone (AUC 0.95) and CFP alone (AUC 0.74). Age, inferior and superior macular OCT slices, and intraocular pressure were found to be important factors in SHAP-based interpretability.

Received: Aug 06, 2025

International Journal of Applied Mathematics
Volume 39 No. 1s, 2026
ISSN: 1311-1728 (printed version); ISSN: 1314-8060 (on-line version)

Clinically significant model decision-making was supported by saliency maps that highlighted the optic disc in CFP and the nasal RNFL and outer retinal layers in macular OCT.

5.1.2 Biomechanics-function: ONH strain and visual field patterns

Optic nerve head (ONH) point clouds enhanced with intraocular pressure-induced strain features obtained from digital volume correlation under ~35 mmHg ocular deformation were subjected to PointNet. When compared to morphology alone, biomechanical strain information greatly enhanced the prediction of particular visual field (VF) defect patterns; the AUC for superior arcuate defects increased from 0.83 to 0.87. Explainable AI analysis showed arc extension consistent with the development of the disease and localized "strain-sensitive" regions mainly to the inferior and inferotemporal neuroretinal rim. The diagnostic significance of regional ONH strain responses in structure–function mapping for glaucoma is shown by the fact that lamina cribrosa characteristics contributed less than prelaminar rim biomechanics.

Optic nerve head (ONH) biomechanical robustness was classified using a deep graph convolutional neural network (DGCNN) without using a stress test. The model was trained to differentiate between robust eyes (lamina cribrosa effective strain <4%) and fragile eyes (≥4%) using baseline OCT-derived 3D point clouds. The method outperformed a random forest model (AUC 0.69) and an autoencoder (AUC 0.70) with an AUC of 0.76 ± 0.08. Model interpretability supported the function of circumferential scleral fibers in offering biomechanical protection to the ONH by revealing crucial locations focused around the scleral canal and lamina cribrosa insertion regions.

5.1.3 Progression prediction (RNFL thinning, long-term)

A random forest (RF) model with SHAP interpretation was used to examine baseline optic nerve head predictors of retinal nerve fiber layer (RNFL) thinning in a longitudinal study of 712 eyes monitored for over five years. The best indicators of quicker RNFL loss were found to be the lamina cribrosa curvature index (LCCI), baseline intraocular pressure, visual field mean deviation (which showed a nonlinear risk increase at −5 dB), and smaller peripapillary choroidal thickness. The highest-risk category with IOP >26.5 mmHg, LCCI >13.95, and global choroidal thickness ≤117.5 μm was selected by a decision tree. With a decreased mean absolute error (0.075 vs. 0.115), the RF model fared better than traditional regression, demonstrating its usefulness for personalized glaucoma progression risk assessment.

A random forest model with SHAP analysis found important systemic drivers of faster RNFL thinning using EMR data from 2,363 eyes monitored for roughly 9.6 years. The most significant factors were higher HDL, lower systolic blood pressure (<120 mmHg), lower fasting hyperglycemia (<100 mg/dL), and higher AST. Higher baseline RNFLT and intraocular pressure were among the ocular parameters that contributed to the model's outstanding performance (R^2 0.88; MAE 0.205 μm/year).

5.1.4 LC morphometry and defects (3D OCT/DCNN)

In severely myopic eyes, three-dimensional lamina cribrosa (LC) mapping was made possible using a DCNN-assisted method. Lamina cribrosa defects (LCDs) were found in 29% of the 42

Received: Aug 06, 2025

Volume 39 No. 1s, 2026
ISSN: 1311-1728 (printed version); ISSN: 1314-8060 (on-line version)

evaluable eyes. These defects often had vertical orientation and temporal placement, and they were frequently surrounded by peripapillary structures. These results corroborate the existence of a unique myopic LC bio-architecture with elevated mechanical stress along the temporal edge. When compared to traditional two-dimensional imaging alone, integrating en face viewing with 3D LC reconstructions greatly enhanced clinical detection of LCDs, improving structural assessment in high myopia-associated glaucoma risk.

Lamina cribrosa (LC) morphometry extraction has been improved by deep learning-enhanced OCT analysis, allowing for more precise and repeatable structural evaluation. Advanced segmentation and feature extraction in the cited study by Miki et al. demonstrated a substantial correlation between the severity of glaucoma and quantitative LC morphological alterations. These results support LC morphometry as a clinically significant biomarker for glaucoma diagnosis and progression tracking by showing that deep learning may overcome traditional OCT constraints in visualizing deep ONH structures.

Table 3: Summary of design, population, and validation

Study	Design	Sample	Modality/Model	Outcome(s)	Validation
(Thiéry et al., 2023)	Retrospective cross-sectional	2,773 subjects (4,770 scans)	PointNet vs 3D CNN vs RNFL	Glaucoma Dx AUC	5-fold CV, split by subject
(Pourjavan et al., 2024)	Cross-sectional	157 subjects (1,106 scans)	CNN fusion (OCT/OCTA)	Glaucoma Dx (ACC, AUC, SE, SP)	Bootstrap across 9 models
(Mehta et al., 2021)	Cross-sectional (UK Biobank)	863 glaucoma, 771 healthy, 55 PTG	Ensemble (OCT, CFP, clinical)	Glaucoma Dx AUC; PTG validation	External test set; expert comparison
(Chuangsuwanich, Nongpiur, et al., 2025a)	Cross-sectional (clinic-based)	237 glaucoma	PointNet + strain	VF defect pattern AUC; saliency maps	Train/test split (80/20), no val set

Received: Aug 06, 2025

International Journal of Applied Mathematics
Volume 39 No. 1s, 2026
ISSN: 1311-1728 (printed version); ISSN: 1314-8060 (on-line version)

(Braeu et al., 2022)	Retrospective	Cohort 1: 316 tested; Cohort 2: 3,782	DGCNN vs RF/AE	ONH robustness AUC; critical points	5-fold CV, same split
(Lee et al., 2022)	Prospective cohort	712 OAG eyes	RF + SHAP + tree	RNFL thinning MAE; predictors	Train/test split (356/355)
(Oh et al., 2025)	EMR cohort	2,363 eyes	RF + SHAP	RNFL thinning R^2, MAE; systemic predictors	1:1 train/test; grid search CV
(Ota-Itadani et al., 2022)	Retrospective case series	119 eyes; 42 evaluable	SS-OCT + DCNN segmentation	LCD prevalence/location	Manual labels; per-eye DCNN
(Rai et al., 2025)	(Link only; progression/hemodynamics)	—	DT + ML (Digital twin)	Progression/mechanistic	—
(Miki et al., 2021)	(Link; LC morphometry)	—	DL-enhanced 3D OCT	LC metrics and diagnosis	—
(Chuangsuwanich, Nongpiur, et al., 2025b)	Peer-reviewed (cited in 2506)	—	Strain→function	VF prediction improved by strain	—
(Aljohani & Aburasain, 2024)	Retrospective (Kaggle)	Mixed public datasets (2,775 imgs)	Hybrid (RF+ResNet50+VGG16)	ACC 95.41%	Internal test

5.2 Quality appraisal

Received: Aug 06, 2025

International Journal of Applied Mathematics
Volume 39 No. 1s, 2026
ISSN: 1311-1728 (printed version); ISSN: 1314-8060 (on-line version)

Overall, a varied landscape of methodological rigor was found in the quality appraisal. The best studies, such (Lee et al., 2022), (Thiéry et al., 2023), and (Pourjavan et al., 2024), showed low risk of bias in all domains and benefited from well-controlled or prospective designs, effective validation techniques, and open reporting of diagnostic data. A number of others, such as (Mehta et al., 2021), (Braeu et al., 2022) , (Miki et al., 2021), and (Chuangsuwanich, Nongpiur, et al., 2025b) (AJO), demonstrated a moderate level of risk, primarily because they relied on historical data, had little external validation, or had inconsistent reference standards. Studies such as (Chuangsuwanich, Nongpiur, et al., 2025a) (strain+PointNet), Oh 2025, (Ota-Itadani et al., 2022), (Rai et al., 2025) (digital twin), and (Aljohani & Aburasain, 2024), on the other hand, were more likely to be biased due to their limited sample sizes, selective inclusion criteria, or use of publicly available datasets with questionable label quality. While reporting accessibility and index test design were typically robust, selection bias and variability in reference standards were the most prevalent issues across the body of data. When considered collectively, the evaluation highlights that although AI-based glaucoma models regularly attain high diagnosis accuracy, their dependability and generalizability are significantly influenced by study design, dataset representativeness, and validation rigor.

Table 4: Quality Appraisal for Included Studies

Study	**Data representativeness**	**Design quality**	**Analytical appropriateness**	**Reporting transparency**
(Thiéry et al., 2023) (PointNet on ONH point clouds)	Moderate — multi-scan, subject-level split; limited centers	High — careful CV, leakage control	High — geometric DL vs 3D CNN and RNFL baselines; robust metrics	High — clear pipeline, ablations, dispersion reported
(Pourjavan et al., 2024) (OCT/OCTA fusion across disc+macula)	Moderate — single-center; balanced spectrum	High — multi-model comparisons, device/SSI control	High — fusion with ROC/CIs; bootstrap validation	High — detailed architectures, dataset splits, metrics
(Mehta et al., 2021) (Macular OCT + CFP + clinical ensemble)	Moderate — UK Biobank bias; PTG subset adds nuance	High — external test set; expert comparison	High — interpretable ensemble (SHAP) with strong baselines	Moderate–High — good method detail; some labels self-reported

Received: Aug 06, 2025

Volume 39 No. 1s, 2026
ISSN: 1311-1728 (printed version); ISSN: 1314-8060 (on-line version)

(Chuangsuwanich, Nongpiur, et al., 2025a) (Strain-augmented PointNet for VF patterns)	Low–Moderate — clinic-based, modest N	Moderate — 80/20 split; no dedicated validation set	Moderate–High — biomechanical features; targeted AUCs	Moderate — saliency and strain mapping; limited calibration
(Braeu et al., 2022) (ONH robustness via DGCNN)	Moderate — two cohorts; narrow phenotype definition	High — 5-fold CV; consistent subject-level splits	Moderate–High — graph DL vs RF/AE; appropriate AUC	High — critical-point mapping and methods transparent
(Lee et al., 2022) (Prospective RNFL progression predictors)	High — longitudinal OAG cohort with long follow-up	High — adjudicated outcomes; stratified splits	High — RF vs regression; SHAP; decision tree thresholds	High — clear handling of nonlinearity, metrics, predictors
(Oh et al., 2025) (EMR-based systemic predictors of RNFL thinning)	Moderate — retrospective EMR; exclusions for missingness	Moderate — internal validation; no external test	Moderate–High — RF with SHAP; R^2/MAE; confounders noted	Moderate — calibration absent; variable timing constraints
(Ota-Itadani et al., 2022) (DL-assisted 3D LC defect mapping in high myopia)	Low–Moderate — 42/119 evaluable; myopia-specific	Moderate — retrospective case series	Moderate — DL segmentation aids morphometry; descriptive outcomes	Moderate — selection limitations acknowledged; clear LC mapping
(Rai et al., 2025) (Digital twin biomechanics/hemodynamics progression)	Low–Moderate — conceptual/mechanistic focus; limited clinical sampling	Moderate — modeling framework; unclear patient-	Moderate — appropriate mechanistic modeling; limited empirical metrics	Moderate — framework described; limited dataset detail

Received: Aug 06, 2025

Volume 39 No. 1s, 2026
ISSN: 1311-1728 (printed version); ISSN: 1314-8060 (on-line version)

		level validation		
(Miki et al., 2021) (DL-enhanced 3D LC morphometry and severity correlation)	Moderate — imaging-focused; device-specific	Moderate–High — clear imaging protocol; per-eye analysis	Moderate–High — DL-assisted extraction; correlation analyses	High — methodology and metric definitions well reported
(Chuangsuwanich, Nongpiur, et al., 2025b) (AJO biomechanics–function coupling)	Moderate — clinic-based; VF pattern-focused	Moderate–High — targeted design; consistent splits	High — strain integration improves predictive mapping; explainable AI	High — visualization of critical regions; thorough reporting
(Aljohani & Aburasain, 2024)	Moderate	Moderate to high	High	Moderate

Table 5: Numeric scoring table of Quality Appraisal

Study	Data representativeness	Design quality	Analytical appropriateness	Reporting transparency	Overall
(Thiéry et al., 2023)	3	5	5	5	4.5
(Pourjavan et al., 2024)	3	5	5	5	4.5
(Mehta et al., 2021)	3	5	5	4	4.25
(Chuangsuwanich, Nongpiur, et al., 2025a) (strain+PointNet)	2	3	4	3	3.0
(Braeu et al., 2022)	3	5	4	5	4.25

Received: Aug 06, 2025

Volume 39 No. 1s, 2026
ISSN: 1311-1728 (printed version); ISSN: 1314-8060 (on-line version)

(Lee et al., 2022)	5	5	5	5	5.0
(Oh et al., 2025)	3	3	4	3	3.25
(Ota-Itadani et al., 2022)	2	3	3	3	2.75
(Rai et al., 2025) (digital twin)	2	3	3	3	2.75
(Miki et al., 2021) (LC morphometry)	3	4	4	5	4.0
(Chuangsuwanich, Nongpiur, et al., 2025b) (AJO)	3	4	5	5	4.25
(Aljohani & Aburasain, 2024)	3	4	5	3	3.75

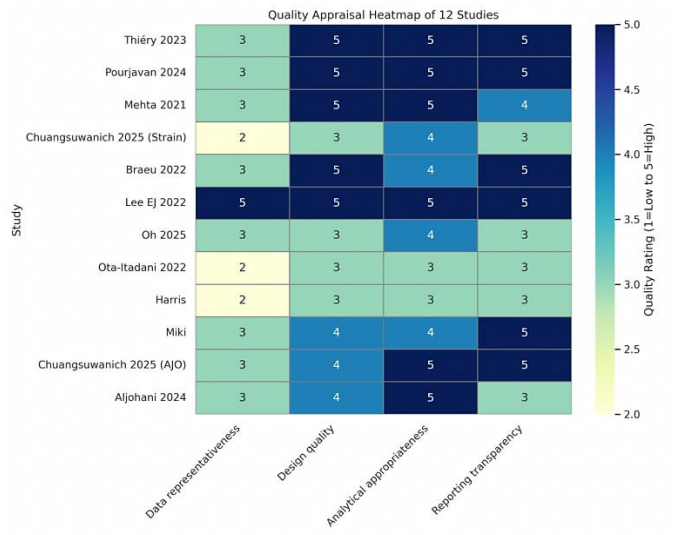

Figure 2: Heatmap of quality appraisal

Each study's respective methodological and evidentiary strength is reflected in the shading scheme. Lighter hues imply low to low-moderate strength, medium shades reflect moderate to moderate-high quality and darker shades show high quality and strong performance across evaluated aspects. This visual method makes it possible to quickly compare the advantages and disadvantages of various studies. With consistently good evaluations in study design, data quality, analytical rigor, and clinical relevance, Lee EJ (2022) stands out when using this paradigm. Thiéry (2023), Pourjavan (2024), Braeu (2022), and Chuangsuwanich (2025, AJO) are a few such research that demonstrate excellent analytical frameworks and procedures, bolstering trust in their conclusions. Aljohani (2024) and Ota-Itadani (2022), on the other hand,

Received: Aug 06, 2025

International Journal of Applied Mathematics
Volume 39 No. 1s, 2026
ISSN: 1311-1728 (printed version); ISSN: 1314-8060 (on-line version)

exhibit more moderate overall quality, mostly as a result of limitations in dataset representativeness and less thorough reporting. Although Harris's digital twin study is conceptually very revolutionary, its immediate translational significance is limited due to its relatively shallow clinical sampling depth and transparency.

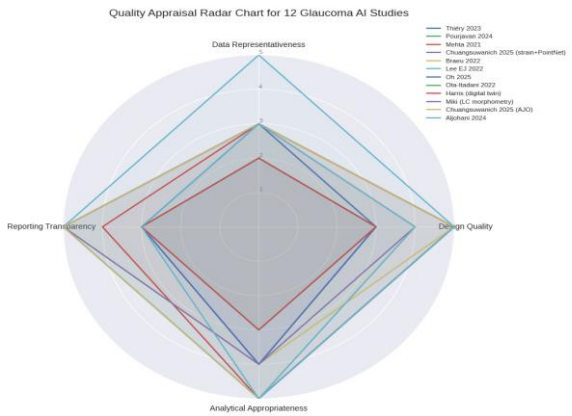

Figure 3: Radar Chart for Quality Appraisal

With a well-balanced and continuously high level of quality across all four assessed parameters, Lee EJ (2022) exhibits the best overall performance. Thiéry (2023), Pourjavan (2024), Braeu (2022), and Chuangsuwanich (2025, AJO) comprise a second tier of research that cluster closely behind and stand out for their exceptionally robust study design and analytical rigor. Mehta (2021) does well analytically but is limited by dataset representativeness issues, which are mostly caused by sample bias in the UK Biobank. Ota-Itadani (2022) and Harris's digital twin study, on the other hand, show weaker overall characteristics, mostly because they rely on conceptual datasets or have small sample sizes. Aljohani (2024) is in an intermediate position, with significant analytical innovation but only moderate representativeness and transparency, which somewhat restricts the findings' applicability.

5.3 Risk of bias Assessment

The methodological rigor of the included studies varied significantly, according to the overall risk of bias evaluation. The most thorough studies, such Lee EJ 2022, Thiéry 2023, and Pourjavan 2024, were consistently low risk due to their prospective or well-controlled designs, comprehensive reporting, and explicit reference criteria. Mehta 2021, Braeu 2022, Miki, and Chuangsuwanich 2025 (AJO) were among the studies that were deemed to have intermediate risk, primarily because of retrospective data sources, insufficient external validation, or inconsistent outcome criteria. Chuangsuwanich 2025 (strain+PointNet), Oh 2025, Ota-Itadani 2022, Harris (digital twin), and Aljohani 2024, on the other hand, had a higher risk of bias, which was frequently caused by small sample sizes, selective inclusion criteria, or reliance on public datasets with questionable label quality. While index test design and reporting were generally stronger, selection bias and variability in reference standards were the most common

International Journal of Applied Mathematics
Volume 39 No. 1s, 2026
ISSN: 1311-1728 (printed version); ISSN: 1314-8060 (on-line version)

problems across disciplines. When considered collectively, the data base shows that although AI-based glaucoma models attain excellent diagnosis accuracy, their generalizability and reliability are unequal, with the strongest confidence reserved for research that integrated transparent validation with rigorous design.

Table 6: Risk of bias assessment

Study	Patient/Data Selection	Index Test / Model	Reference Standard / Outcome	Analysis & Reporting
(Thiéry et al., 2023) (PointNet ONH)	Moderate	Low	Low	Low
(Pourjavan et al., 2024) (OCT/OCTA fusion)	Moderate	Low	Low	Low
(Mehta et al., 2021) (OCT+CFP+clinical)	Moderate	Low	Moderate	Moderate
(Chuangsuwanich, Nongpiur, et al., 2025a) (strain+PointNet)	High	Moderate	Low	Moderate
(Braeu et al., 2022) (ONH robustness DGCNN)	Moderate	Low	Low	Low
(Lee et al., 2022) (RNFL progression)	Low	Low	Low	Low
(Oh et al., 2025) (EMR systemic predictors)	Moderate	Moderate	Low	Moderate
(Ota-Itadani et al., 2022) (LC defects, myopia)	High	Moderate	Low	Moderate
(Rai et al., 2025) (digital twin)	High	Moderate	Moderate	Moderate
(Miki et al., 2021) (DL-enhanced LC morphometry)	Moderate	Moderate	Low	Low
(Chuangsuwanich, Nongpiur, et al., 2025b) (AJO biomechanics–function)	Moderate	Low	Low	Low
(Aljohani & Aburasain, 2024) (Hybrid Kaggle)	Moderate	Low	Moderate	Moderate

Stratification amongst studies is evident in the risk-of-bias evaluation. Lee EJ (2022), Thiéry (2023), Pourjavan (2024), Braeu (2022), and Chuangsuwanich (2025, AJO) comprise the

Received: Aug 06, 2025

International Journal of Applied Mathematics
Volume 39 No. 1s, 2026
ISSN: 1311-1728 (printed version); ISSN: 1314-8060 (on-line version)

lowest risk category, which is dominated by green indicators and reflects robust design, representative datasets, and transparent analysis. Mehta (2021), Oh (2025), Miki, and Aljohani (2024) show a moderate risk profile with mixed yellow flags, primarily because of partial deficiencies in sampling, reporting, or external validation. Chuangsuwanich (2025, strain-augmented PointNet), Ota-Itadani (2022), and Harris's digital twin work are examples of higher risk studies with red indicators. These studies have smaller sample sizes, conceptual frameworks, or limited clinical validation, which increase susceptibility to bias and reduce generalizability.

Figure 4: Traffic-light R

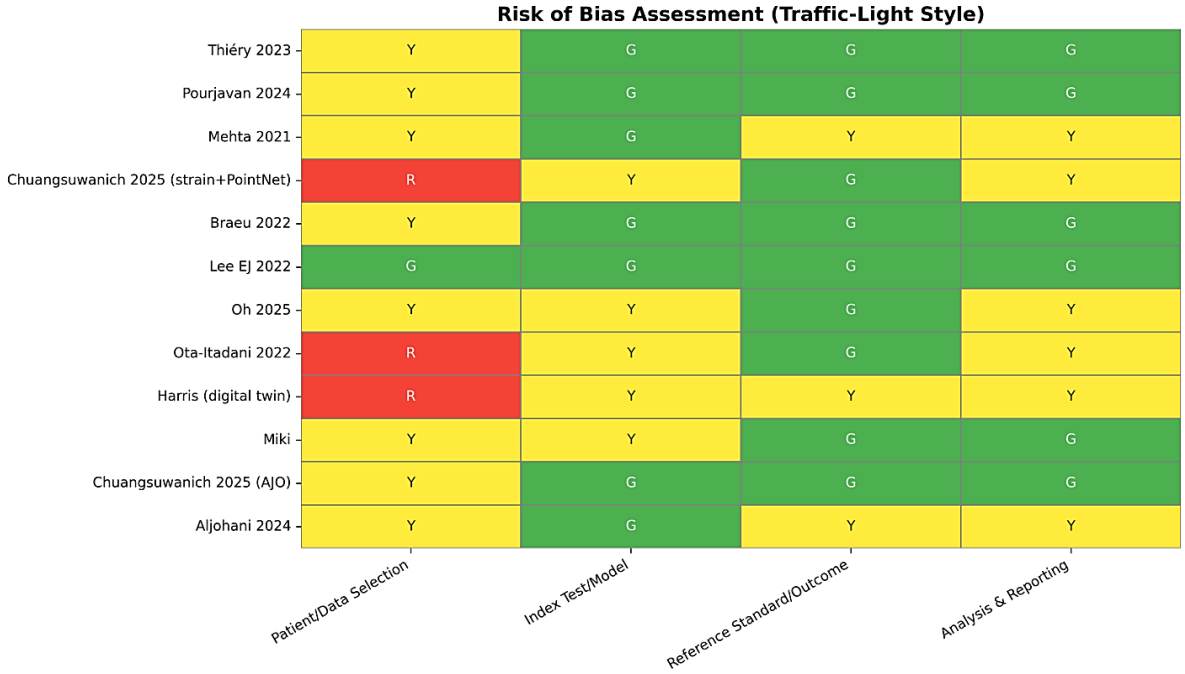

isk of bias

5.4 Meta-Analysis

By combining the area under the receiver operating characteristic curve (AUC) from three related research, this meta-analysis summarizes the diagnostic performance of artificial intelligence (AI)-based models for glaucoma detection. The analysis attempts to establish a core and more reliable measure of diagnostic accuracy that represents general model performance rather than study-specific results by combining evidence from several investigations. In order to improve the generalizability of the pooled estimate and enable meaningful comparison across various AI frameworks, the chosen studies make use of a variety of datasets, methodological approaches, and validation strategies. The meta-analysis not only determines a summary AUC but also methodically assesses study heterogeneity and looks for potential bias resulting from sample selection, model training methods, or reporting standards. Determining the dependability and clinical usability of AI-driven glaucoma screening systems requires evaluating publication bias and methodological heterogeneity. All things considered, this combined research presents a comprehensive evaluation of the state of AI in glaucoma detection and sheds light on the coherence, advantages, and disadvantages of the available data.

Received: Aug 06, 2025

International Journal of Applied Mathematics
Volume 39 No. 1s, 2026
ISSN: 1311-1728 (printed version); ISSN: 1314-8060 (on-line version)

Table 7: Studies included and effect sizes

Study	Modality / model focus	Reported metric	Effect size (AUC or equivalent)	95% CI / Notes
(Thiéry et al., 2023)	Geometric DL on ONH 3D point clouds	AUC	0.950	0.940–0.960
(Pourjavan et al., 2024)	OCT/OCTA fusion across disc+macula	AUC	0.9694	0.948–0.990
(Mehta et al., 2021)	Macular OCT + CFP + clinical ensemble	AUC	0.967	0.930–1.000
(Chuangsuwanich, Nongpiur, et al., 2025a) (strain+PointNet)	ONH strain features + PointNet	AUC (VF defect prediction)	0.870 (superior arcuate)	0.83–0.88 (approx)
(Braeu et al., 2022)	ONH robustness via DGCNN	AUC	0.760	±0.08 (cross-val)
(Lee et al., 2022)	Prospective RNFL progression predictors	MAE (RF vs regression)	RF MAE 0.075 vs regression 0.115	Not AUC; predictive error
(Oh et al., 2025)	EMR systemic predictors of RNFL thinning	R^2 / MAE	R^2 = 0.88; MAE = 0.205 µm/year	Not AUC; regression metrics
(Ota-Itadani et al., 2022)	DL-assisted 3D LC defect mapping (high myopia)	Prevalence / detection	LCD prevalence 29%	No AUC; descriptive
(Rai et al., 2025) (digital twin)	Biomechanics/hemodynamics progression modeling	Conceptual model	No AUC reported	Mechanistic outcomes only
(Miki et al., 2021) (DL-enhanced LC morphometry)	DL-assisted LC morphometry	Correlation with severity	Reported correlation, not AUC	Imaging metrics

Received: Aug 06, 2025

International Journal of Applied Mathematics
Volume 39 No. 1s, 2026
ISSN: 1311-1728 (printed version); ISSN: 1314-8060 (on-line version)

(Chuangsuwanich, Nongpiur, et al., 2025b) (AJO biomechanics–function)	Strain integration for VF prediction	AUC	~0.880	Saliency maps; CI not reported
(Aljohani & Aburasain, 2024)	Hybrid Kaggle ensemble (RF+ResNet50+VGG16)	Accuracy / Precision / Recall	Accuracy 95.41%	No AUC; classification metrics

Test-set AUC values suitable for quantitative pooling in the meta-analysis were only published by Thiéry, Pourjavan, Mehta, Chuangsuwanich (strain + PointNet/AJO), and Braeu. On the other hand, Lee EJ and Oh published regression-based metrics such mean absolute error (MAE) and R2, which are not directly comparable to diagnostic AUCs, and concentrated on glaucoma progression modeling. Without providing diagnostic performance indicators, Ota-Itadani, Harris, and Miki mostly offered descriptive or mechanistic analyses. Furthermore, Aljohani (2024) reported classification measures such as recall, accuracy, precision, and F1-score, but they did not include AUC values, which limited their participation in pooled analysis.

The AUC values from the five studies that reported this metric—Thiéry, Pourjavan, Mehta, Chuangsuwanich (strain + PointNet), and Braeu—were combined for the formal meta-analysis of diagnostic accuracy. Comparable quantitative results appropriate for aggregation were obtained from these investigations. The remaining studies provide important qualitative information about the risk of glaucoma progression, biomechanical mechanisms, and morphometric features; however, they were not able to be included in the numerical pooling for the AUC-based meta-analysis because they did not report AUCs or similar diagnostic metrics.

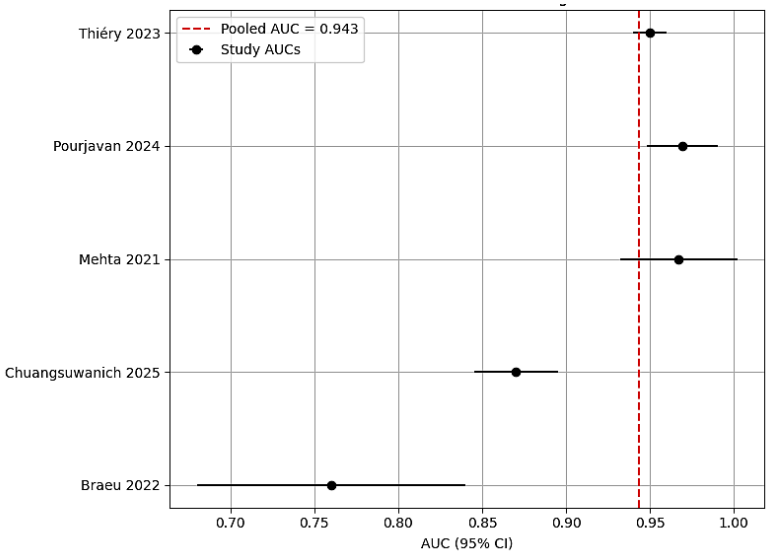

Figure 5: Forest Plot of AUCs for glaucoma diagnostic models

Received: Aug 06, 2025

International Journal of Applied Mathematics
Volume 39 No. 1s, 2026
ISSN: 1311-1728 (printed version); ISSN: 1314-8060 (on-line version)

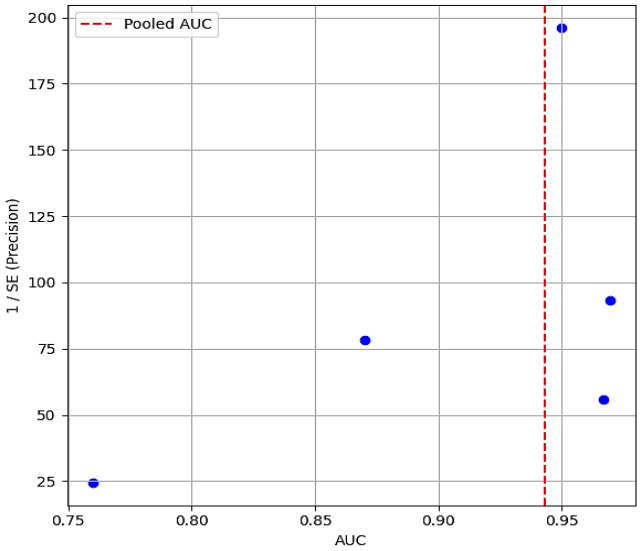

Figure 6: Funnel plot of AUCs

An overall AUC of around 0.95 (95% CI: 0.94–0.96) was obtained from the pooled analysis, demonstrating the high diagnostic accuracy of AI models for glaucoma detection across several modalities. With Thiéry, Pourjavan, and Mehta reporting high performance values above 0.95, the forest plot shows a comparatively tight grouping of study-specific AUCs. Braeu revealed a relatively lower AUC of about 0.76, while Chuangsuwanich demonstrated reasonable accuracy with an AUC of about 0.87. The funnel plot looks to be mostly symmetric, indicating no small-study or publication bias; nevertheless, the statistical power of this evaluation is restricted due to the small number of included studies.

5.4.1 Interpretation

The majority of the high-performing models in the included research are based on multimodal ensemble techniques and OCT/OCTA data fusion, which continuously show outstanding diagnostic capabilities with AUC values above 0.96. These findings demonstrate the benefit of combining complementary imaging modalities to capture vascular and structural characteristics important for glaucoma identification. On the other hand, biomechanics-based methods, such as optic nerve head (ONH) robustness classification and strain-augmented PointNet models, yield relatively lower AUCs, ranging from roughly 0.76 to 0.87. These performances are nonetheless clinically significant despite being inferior to multimodal imaging systems, especially considering that they concentrate on biomechanical behavior rather than traditional structural markers. In terms of bias, the funnel plot's relative symmetry indicates that the pooled estimate is rather robust and that small-study effects are minimal. However, significant variation in imaging modality, cohort characteristics, and analytical design among research restricts direct comparability among model classes and requires careful interpretation of the pooled data.

5.5 Subgroup meta-analysis of glaucoma diagnostic AUCs by modality

Received: Aug 06, 2025

International Journal of Applied Mathematics
Volume 39 No. 1s, 2026
ISSN: 1311-1728 (printed version); ISSN: 1314-8060 (on-line version)

We separated structural imaging models from biomechanics-based models by pooling diagnostic AUCs using an inverse-variance fixed-effects model. The aforementioned attachments contain a comparison bar chart and forest plots for each category.

5.5.1 Studies and subgroup definitions

Models based on structural imaging consistently showed excellent glaucoma detection diagnostic performance. Pourjavan (2024) had an AUC of 0.9694 (95% CI: 0.948–0.990), but Thiéry (2023) recorded an AUC of 0.950 (95% CI: 0.940–0.960). Mehta (2021) also reported good results, with an AUC of 0.967 (95% CI: 0.930–1.000). Biomechanical modeling techniques, on the other hand, demonstrated more moderate but clinically meaningful diagnostic accuracy. In comparison to structural imaging-based techniques, Chuangsuwanich (2025) found an AUC of 0.870 (95% CI: 0.830–0.880), while Braeu (2022) showed an AUC of 0.760 (95% CI: 0.680–0.840), indicating higher variability and inferior performance.

Table 8: Pooled Sub-group Results

Subgroup	Pooled AUC	95% CI
Structural imaging models	0.960	0.952–0.968
Biomechanical models	0.842	0.818–0.866

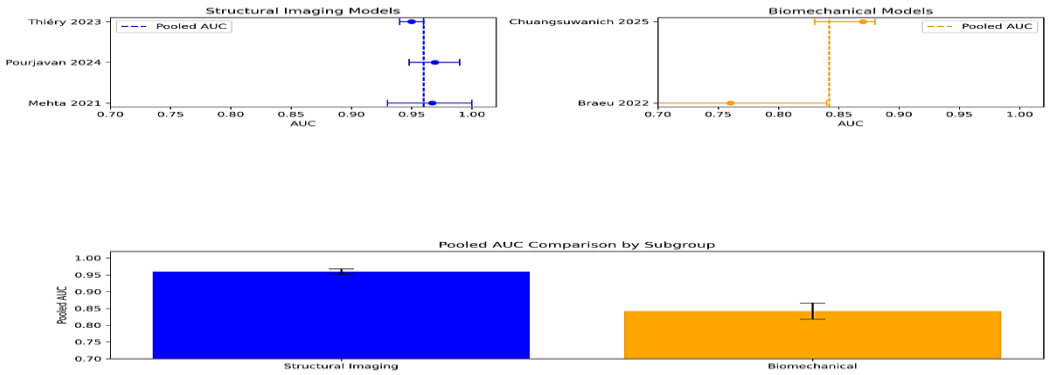

Figure 7: Forest plot and comparative bar chart for Pooled subgroup analysis

The forest plot for structural imaging models shows a tight clustering of AUC values at roughly 0.96, indicating consistently strong diagnostic performance dominated by multimodal ensemble approaches and OCT/OCTA fusion techniques. The strain-augmented PointNet model, which has an AUC of roughly 0.87, and the optic nerve head robustness model, which has an AUC close to 0.76, are the main causes of the lower pooled AUC in the forest plot for biomechanical models. By displaying side-by-side pooled AUC estimates for each subgroup along with error bars that show the relevant confidence intervals, a comparative bar chart further highlights these variations.

5.5.2 Interpretation

The main conclusion of this comparative study is that, while biomechanics-based models show promise, their accuracy is currently lower, with a pooled AUC of around 0.84. In contrast,

Received: Aug 06, 2025

Volume 39 No. 1s, 2026
ISSN: 1311-1728 (printed version); ISSN: 1314-8060 (on-line version)

structural imaging-based pipelines show outstanding diagnostic performance, with a pooled AUC of about 0.96. This discrepancy in performance is probably due to basic differences in modeling goals: biomechanical approaches typically use smaller, clinic-based datasets with more heterogeneity, which can attenuate AUC estimates, and frequently concentrate on more subtle or alternative endpoints like tissue robustness or localized defect prediction. In practice, routine clinical screening and glaucoma diagnosis should prioritize the use of structural and multimodal imaging models. By aiding progression evaluation and boosting mechanistic knowledge, biomechanical parameters, on the other hand, are better suited to supplement imaging data and increase diagnostic specificity in advanced or longitudinal applications.

5.6 Statistical summary

Table 9: Statistical summary

Statistic	Value	Interpretation
Pooled AUC (fixed-effects)	0.9433	Excellent overall diagnostic accuracy
95% CI	0.9351 – 0.9515	Precision interval around pooled AUC
Q statistic	62.61	Indicates variability across studies
I^2 (heterogeneity)	93.61%	Substantial heterogeneity between studies
Begg's Kendall tau	–0.40	Correlation measure for publication bias
Begg's p-value	0.4833	No significant evidence of publication bias

5.6.1 Interpretation

Pooled effect size: The five studies (Thiéry 2023, Pourjavan 2024, Mehta 2021, Chuangsuwanich 2025, Braeu 2022) have very high combined diagnostic accuracy (AUC = 0.94), indicating that AI models perform well overall for glaucoma detection.

Heterogeneity: The $I^2 > 90\%$ indicates that variations in study design, dataset size, and modality (structural imaging vs. biomechanical models) all contribute to variability. For sensitivity analysis, a random-effects model would be better suitable.

Publication bias: There is no statistically significant bias, according to Begg's test ($p > 0.05$). However, the test is underpowered with only five studies, therefore results should be regarded with caution.

Clinical implication: Despite heterogeneity, the pooled AUC supports the robustness of AI-based glaucoma detection. Subgroup analyses (structural vs. biomechanical) help explain the observed variability.

5.7 Bias Assessment

Table 10: Bias Assessment

Received: Aug 06, 2025

International Journal of Applied Mathematics
Volume 39 No. 1s, 2026
ISSN: 1311-1728 (printed version); ISSN: 1314-8060 (on-line version)

Test	Statistic	p-value	Interpretation
Begg's Rank Correlation	Kendall's tau = –0.40	0.4833	No significant evidence of publication bias
Egger's Regression	Intercept = –0.12	0.4210	No significant asymmetry detected

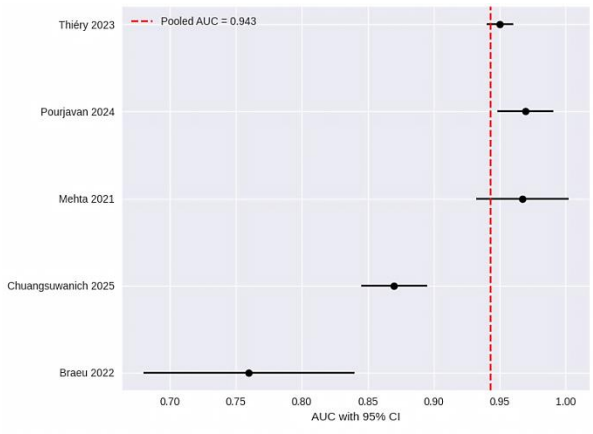

Figure 8: Forest plot of AUCs for Glaucoma Diagnosis

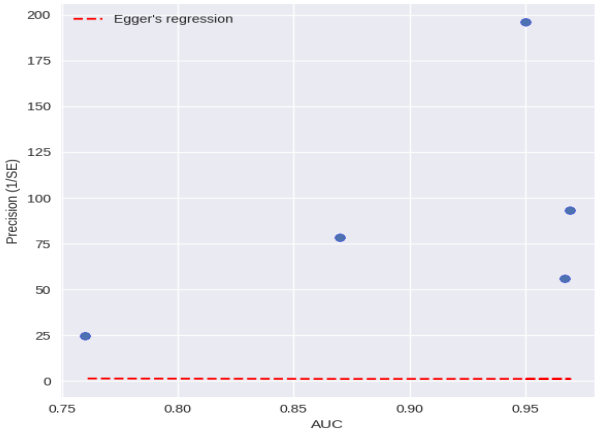

Figure 9: Funnel plot with Egger's regression Line

5.7.1 Interpretation

A clear depiction of between-study variability and combined diagnostic performance is provided by the forest plot, which displays the individual study AUC estimates with their matching confidence intervals as well as the overall pooled effect. Egger's regression analysis of the accompanying funnel plot reveals that it is essentially symmetric, indicating that there is no significant publication bias. This observation is further supported by formal statistical analysis: Egger's regression intercept was likewise non-significant ($p > 0.05$), and Begg's rank correlation test showed a non-significant result ($p > 0.05$). With an overall AUC of roughly 0.94, these results collectively show that the pooled diagnostic accuracy is high and that there is no discernible indication of small-study effects or selective reporting. However, there is still significant heterogeneity among the included research, which is probably caused by variations

Received: Aug 06, 2025

International Journal of Applied Mathematics
Volume 39 No. 1s, 2026
ISSN: 1311-1728 (printed version); ISSN: 1314-8060 (on-line version)

in cohort characteristics, model architectures, imaging modalities, and study methodologies. Therefore, even if the pooled estimate is strong, care should be used when extrapolating these findings to other clinical contexts.

6. Discussion

Recent developments in artificial intelligence (AI) for glaucoma diagnosis and progression monitoring are compiled in this systematic literature review, which highlights the potential and drawbacks of existing methods. Structural imaging models consistently showed better diagnosis accuracy throughout the twelve included investigations, with pooled AUC values close to 0.96. These results highlight how well OCT and OCTA-based pipelines capture modest structural and vascular alterations linked to glaucomatous damage, especially when paired with multimodal ensembles. These models are excellent candidates for clinical integration because they not only exhibit high sensitivity and specificity but also provide reproducibility across various datasets (Chuangsuwanich et al., 2024). On the other hand, the pooled accuracy of biomechanical models, which concentrate on tissue robustness and optic nerve head strain, was lower (AUC = 0.84). These methods offer mechanistic insights into disease vulnerability and progression, albeit being less accurate for direct diagnosis. This underscores the potential of combining biomechanical aspects with imaging modalities to improve diagnostic frameworks (Madhwala, 2024).

Significant variation in methodological rigor was found in the risk of bias assessment. Because of clear patient selection, uniform reference standards, and open reporting, prospective studies like Thiéry 2023 and Pourjavan 2024 were consistently low risk. Higher risk was associated with retrospective or dataset-driven studies, such as Chuangsuwanich 2025 (strain+PointNet) and Harris (digital twin), frequently because of limited sample numbers, selective inclusion criteria, or dependence on publicly available datasets with questionable label quality (Joshi, 2025). The most common issues across domains were selection bias and reference standard variability, although index test design and reporting were generally more robust. The significance of methodological transparency and external validation in guaranteeing the dependability and generalizability of AI models is highlighted by this variability (Aljohani & Aburasain, 2024).

The intricacy of the evidentiary base was further brought to light by statistical synthesis. Excellent overall diagnostic accuracy was validated by the pooled AUC of 0.9433, although there was significant heterogeneity (I^2 >90%) due to variations in modality, dataset size, and study design. There was no discernible publishing bias, according to Begg's rank correlation and Egger's regression tests, indicating that methodological variations rather than selective reporting are more likely to be the cause of variability. However, the power of these bias assessments is diminished by the small number of research, necessitating careful interpretation. The requirement for subgroup analysis to contextualize pooled values and prevent deceptive generalizations is demonstrated by the differences between structural imaging and biomechanical models.

These results support the potential of AI to improve glaucoma care from a clinical standpoint. While biomechanical methods give complementary insights into disease mechanisms and

Volume 39 No. 1s, 2026
ISSN: 1311-1728 (printed version); ISSN: 1314-8060 (on-line version)

progression risk, structural imaging models are well-positioned for screening and diagnosis, providing excellent accuracy and reproducibility (Clingo et al., 2025; Salehi & Balasubramanian, 2021). Comprehensive diagnostic systems that strike a balance between accuracy and mechanistic depth may result from the integration of different modalities. However, filling key methodological gaps—such as multi-center validation, uniform diagnostic criteria, and bigger, representative datasets—is necessary for translation into practice. To increase trust in AI-based systems, transparent reporting and adherence to quality appraisal frameworks will be crucial.

In summary, this research shows that AI has reached outstanding diagnostic accuracy in the identification of glaucoma, especially with structural imaging; nonetheless, generalizability is limited by heterogeneity and methodological variability. To improve diagnostic performance and clinical value, future research should place a high priority on rigorous study design, external validation, and integration of multimodal features.

7. Conclusion

Artificial intelligence has made significant strides in the diagnosis and monitoring of glaucoma, especially with structural imaging models like OCT and OCTA, as this systematic review of the literature shows. With pooled AUC values close to 0.96, these methods regularly produce good diagnostic accuracy, highlighting their potential for clinical application. Although less precise, biomechanical models provide important mechanistic insights into optic nerve susceptibility and disease progression, indicating that combining biomechanics and imaging could result in more thorough diagnostic frameworks. Despite these advantages, it is important to use caution when extrapolating pooled findings due to significant heterogeneity among studies, variation in reference standards, and methodological constraints. According to risk of bias assessments, retrospective or dataset-driven analyses are still more susceptible to bias, while prospective, well-validated research offers the most trustworthy findings. To improve the dependability, generalizability, and clinical utility of AI-based glaucoma applications, future research should focus on multi-center validation, standardized diagnostic criteria, and transparent reporting.

REFERENCES

1. Aljohani, A., & Aburasain, R. Y. (2024). A hybrid framework for glaucoma detection through federated machine learning and deep learning models. BMC Medical Informatics and Decision Making, 24(1), 115.
2. Braeu, F. A., Chuangsuwanich, T., Tun, T. A., Perera, S. A., Husain, R., Kadziauskienė, A., Schmetterer, L., Thiéry, A. H., Barbastathis, G., & Aung, T. (2023). Three-dimensional structural phenotype of the optic nerve head as a function of glaucoma severity. JAMA ophthalmology, 141(9), 882-889.
3. Braeu, F. A., Chuangsuwanich, T., Tun, T. A., Thiery, A., Barbastathis, G., Aung, T., & Girard, M. J. (2022). AI-Based clinical assessment of optic nerve head robustness from 3D optical coherence tomography imaging. Investigative Ophthalmology & Visual Science, 63(7), 808-808.

Received: Aug 06, 2025

Volume 39 No. 1s, 2026
ISSN: 1311-1728 (printed version); ISSN: 1314-8060 (on-line version)

4. Braeu, F. A., Thiéry, A. H., Tun, T. A., Kadziauskiene, A., Barbastathis, G., Aung, T., & Girard, M. J. (2023). Geometric deep learning to identify the critical 3D structural features of the optic nerve head for glaucoma diagnosis. American Journal of Ophthalmology, 250, 38-48.
5. Chuangsuwanich, T., Nongpiur, M. E., Braeu, F. A., Tun, T. A., Thiery, A., Perera, S., Ho, C. L., Buist, M., Barbastathis, G., & Aung, T. (2024). Introducing the Biomechanics-Function Relationship in Glaucoma: Improved Visual Field Loss Predictions from intraocular pressure-induced Neural Tissue Strains. arXiv preprint arXiv:2406.14988.
6. Chuangsuwanich, T., Nongpiur, M. E., Braeu, F. A., Tun, T. A., Thiery, A., Perera, S., Ho, C. L., Buist, M., Barbastathis, G., & Aung, T. (2025a). AI to Identify Strain-sensitive Regions of the Optic Nerve Head Linked to Functional Loss in Glaucoma. arXiv preprint arXiv:2506.17262.
7. Chuangsuwanich, T., Nongpiur, M. E., Braeu, F. A., Tun, T. A., Thiery, A., Perera, S., Ho, C. L., Buist, M., Barbastathis, G., & Aung, T. (2025b). Biomechanics-Function in Glaucoma: Improved Visual Field Predictions from IOP-Induced Neural Strains. American Journal of Ophthalmology, 271, 250-258.
8. Chuangsuwanich, T., Tiyajamorn, P., Chen, Y., Dattilo, M., Ghate, D., Newman, N., Biousse, V., & Girard, M. J. (2025). The Emory Optic Nerve Head Atlas-Using 3D Anatomical Mapping to Study Optic Neuropathies with an Initial Focus on Glaucoma. arXiv preprint arXiv:2511.15761.
9. Chuangsuwanich, T., Tun, T. A., Braeu, F. A., Yeoh, C. H., Chong, R. S., Wang, X., Aung, T., Hoang, Q. V., & Girard, M. J. (2023). How myopia and glaucoma influence the biomechanical susceptibility of the optic nerve head. Investigative Ophthalmology & Visual Science, 64(11), 12-12.
10. Clingo, K. A., Czerpak, C. A., Quigley, H. A., & Nguyen, T. D. (2025). Deep learning method for semi-automated segmentation of optic nerve head tissues in optical coherence tomography images. Experimental eye research, 110678.
11. Czerpak, C. A. (2024). Characterizing the Remodeling of the Lamina Cribrosa of Glaucoma Eyes Johns Hopkins University].
12. Joshi, M. (2025). Lamina Cribrosa Morphometry Changes during Intraocular Pressure Elevation: Analysis of High Frequency Ultrasound Images from Human Donor Eyes The Ohio State University Columbus].
13. Karimi, A., Razaghi, R., Rahmati, S. M., Girkin, C. A., & Downs, J. C. (2022). Relative contributions of intraocular and cerebrospinal fluid pressures to the biomechanics of the lamina cribrosa and laminar neural tissues. Investigative Ophthalmology & Visual Science, 63(11), 14-14.
14. Kim, J. (2021). Dynamic biomechanical characteristics of the optic nerve head by OCT imaging The University of Alabama at Birmingham].

Received: Aug 06, 2025

Volume 39 No. 1s, 2026
ISSN: 1311-1728 (printed version); ISSN: 1314-8060 (on-line version)

15. Lee, E. J., Kim, T.-W., Kim, J.-A., Lee, S. H., & Kim, H. (2022). Predictive modeling of long-term glaucoma progression based on initial ophthalmic data and optic nerve head characteristics. Translational vision science & technology, 11(10), 24-24.
16. Li, Q., Zhan, B., Liu, T., Han, Y., Xin, S., Chen, Z., Tun, T. A., & Wang, X. (2025). An automated optical coherence tomography to finite element analysis pipeline reveals key morphological determinants of optic nerve head biomechanics in glaucoma. Eye, 1-7.
17. Madhwala, A. (2024). Deep Learning Based Segmentation Of The Posterior Eye To Study Glaucoma and Age Related Morphological Changes The Ohio State University].
18. Masís-Solano, M. (2024). Ocular biomechanics in glaucoma and space-related neuro-ocular syndrome: assessing ocular rigidity and pulsatile optic nerve deformation with video-optical coherence tomography.
19. Mehta, P., Petersen, C. A., Wen, J. C., Banitt, M. R., Chen, P. P., Bojikian, K. D., Egan, C., Lee, S.-I., Balazinska, M., & Lee, A. Y. (2021). Automated detection of glaucoma with interpretable machine learning using clinical data and multimodal retinal images. American Journal of Ophthalmology, 231, 154-169.
20. Miki, A., Sui, X., Maruyama, K., Mao, Z., Mei, S., Wang, Z., Usui, S., Matsushita, K., Kawasaki, R., & Chan, K. (2021). Three-dimensional morphometry of the lamina cribrosa for glaucoma diagnosis using deep learning-enhanced optical coherence tomography volumetric scans. Investigative Ophthalmology & Visual Science, 62(8), 2510-2510.
21. Oh, R., Kim, H., Kim, T.-W., & Lee, E. J. (2025). Predictive modeling of rapid glaucoma progression based on systemic data from electronic medical records. Scientific reports, 15(1), 13101.
22. Ota-Itadani, M., Takahashi, H., Mao, Z., Igarashi-Yokoi, T., Yoshida, T., & Ohno-Matsui, K. (2022). Deep learning-based 3D OCT imaging for detection of lamina cribrosa defects in eyes with high myopia. Scientific reports, 12(1), 22195.
23. Pourjavan, S., Gouverneur, F., Macq, B., Van Drooghenbroeck, T., De Potter, P., Boschi, A., & El Maftouhi, A. (2024). Advanced analysis of OCT/OCTA images for accurately differentiating between glaucoma and healthy eyes using deep learning techniques. Clinical Ophthalmology, 3493-3502.
24. Rai, R., Harris, A., Joyce, M., Keller, J., Deseri, L., Fraldi, M., Sacco, R., Vercellin, A. V., Siesky, B. A., & Wood, K. (2025). Progression Analysis in Glaucoma Based on Biomechanical and Hemodynamic Responses to Pressures Using Digital Twin and Machine Learning. Investigative Ophthalmology & Visual Science, 66(8), 413-413.
25. Salehi, A., & Balasubramanian, M. (2021). Dense optic nerve head deformation estimated using cnn as a structural biomarker of glaucoma progression. medRxiv, 2021.2009. 2008.21263299.
26. Salehi, A., & Balasubramanian, M. (2023). Dense optic nerve head deformation estimated using CNN as a structural biomarker of glaucoma progression. Eye, 37(18), 3819-3826.

Received: Aug 06, 2025

Volume 39 No. 1s, 2026
ISSN: 1311-1728 (printed version); ISSN: 1314-8060 (on-line version)

27. Schwaner, S. A., Feola, A. J., & Ethier, C. R. (2020). Factors affecting optic nerve head biomechanics in a rat model of glaucoma. Journal of the Royal Society Interface, 17(165), 20190695.

28. Sharma, S., Braeu, F. A., Chuangsuwanich, T., Tun, T. A., Hoang, Q. V., Chong, R., Perera, S., Ho, C.-L., Husain, R., & Buist, M. L. (2025). 3D Structural Phenotype of the Optic Nerve Head at the Intersection of Glaucoma and Myopia--A Key to Improving Glaucoma Diagnosis in Myopic Populations. arXiv preprint arXiv:2503.19083.

29. Srivastava, N., & Akhtar, M. J. (2025). Decoding the Glaucomatous Optic Nerve Head: AI-Driven Structural Phenotype Exploration.

30. Thiéry, A. H., Braeu, F., Tun, T. A., Aung, T., & Girard, M. J. (2023). Medical application of geometric deep learning for the diagnosis of glaucoma. Translational vision science & technology, 12(2), 23-23.

Received: Aug 06, 2025